Simple and efficient integration of rigid rotations suitable for constraint solvers

Tomasz Koziara, Nenad Bićanić

Department of Civil Engineering
University of Glasgow, Glasgow G12 8LT, UK

Abstract

Simple and efficient way of integrating rigid rotations is presented. The algorithm is stable, second order accurate, and in its explicit version involves evaluation of only two exponential maps per time step. The semi-explicit version of the proposed scheme improves upon the long term stability, while it retains the explicitness in the force evaluation. The algebraic structure of both schemes makes them suitable for the analysis of constrained multi-body systems. The explicit algorithm is specifically aimed at the analysis involving small incremental rotations, where its modest computational cost becomes the major advantage. The semi-explicit scheme naturally broadens the scope of possible applications.

Key words: rigid rotations, time integration, explicit scheme, constrained motion

1 Introduction

In the explicit analysis of constrained multi-body dynamics it is convenient to employ the following time stepping

$$\mathbf{q}^{t+\frac{h}{2}} = \mathbf{q}^t + \frac{h}{2}\mathbf{u}^t \tag{1}$$

$$\mathbf{u}^{t+h} = \mathbf{u}^t + \mathbf{M}^{-1}h\mathbf{f}^{t+\frac{h}{2}} + \mathbf{M}^{-1}\mathbf{H}^T h\Lambda^{t+\frac{h}{2}} \tag{2}$$

$$\mathbf{q}^{t+h} = \mathbf{q}^{t+\frac{h}{2}} + \frac{h}{2}\mathbf{u}^{t+h} \tag{3}$$

Email address: t.koziara@civil.gla.ac.uk, n.bicanic@civil.gla.ac.uk (Tomasz Koziara, Nenad Bićanić).

where $\mathbf{u}$ is a velocity, $\mathbf{q}$ is a configuration, $\mathbf{M}$ is an inertia operator, $\mathbf{f}$ represents a generalised out of balance force, $\mathbf{H}$ incorporates gradients of constraints, and Λ stores the constraints reactions. We refer the reader to [1], Chapter 5 and references therein for a detailed discussion on (1-3). The utility of the above formulae results from several elementary facts

(1) Combination of the central difference scheme and the trapezoidal rule maintains good conservation properties and is second order accurate.
(2) The mid-step configuration $\mathbf{q}^{t+\frac{h}{2}}$ can be utilised for both, calculation of the constraints gradients operator $\mathbf{H}$ and approximation of $\mathbf{f}^{t+\frac{h}{2}}$.
(3) The momentum balance (2) can be employed to calculate the constraints reactions $\Lambda^{t+\frac{h}{2}}$.
(4) If a suitable kinematic formulation is used, the inverse of inertia $\mathbf{M}^{-1}$ is computed only once.

The above scheme is applicable if the velocity and the configuration belong to the same vector space. For rigid rotations this is not the case. From the implementation point of view, it is often suitable to store and update the orthogonal rotation operator $\mathbf{R}$. Motion of a rigid body reads then

$$\mathbf{x}\left(\mathbf{X},t\right)=\mathbf{R}\left(t\right)\left(\mathbf{X}-\bar{\mathbf{X}}\right)+\bar{\mathbf{x}}\left(t\right) \tag{4}$$

where $\mathbf{x}$, $\mathbf{X}$ are the spatial and the referential [1] points, and $\bar{\mathbf{x}}$, $\bar{\mathbf{X}}$ are the spatial and the referential mass centres. The rotation operator can be updated in several alternative ways. For example Simo and Wong [2] use the incremental rotation vector in their explicit algorithm, and the quaternion representation in the implicit scheme presented in the same paper. Many of the recently proposed time stepping algorithms employ the incremental rotation vector [3,4,5].

The main purpose of this paper is to present an explicit time stepping for rigid rotations, that preserves the structure and the advantages of formulae (1-3). In the pursuit of this goal it will be necessary to abuse slightly the notion of *geometrical consistency*, although the resulting self-starting scheme will have qualities of modest computational cost, second order accuracy, and acceptable stability. As an obvious refinement, a semi-explicit scheme is obtained. For the price of an increased computational cost, it offers an improved long term stability and retains the explicitness in the force evaluation.

Section 2 gives some preliminary remarks. Section 3 specifies the proposed scheme. Section 4 comments on the stability. Section 5 summarises enforcements of the constraints. Section 6 briefly comments on efficiency. Section 7

[1] *Referential* and *body-frame* are used interchangeably across the text.

illustrates the performance on several examples. The paper is concluded in Section 8.

2 Preliminaries

Let us refer the reader to the papers by Simo and Wong [2] and by Krysl and Endres [4] for the brief theoretical introduction into the matters of rigid rotations. Several formulae are only recalled here after [2,4] in order to facilitate the reading (formula-specific references are mostly omitted).

We recall, that the orthogonal rotation operator $\mathbf{R}(t)$ belongs to a curved space, the special orthogonal group $SO(3)$. It is updated in the multiplicative manner

$$\mathbf{R}(t+h) = \mathbf{R}(t) \exp[\mathbf{\Psi}(h)] \tag{5}$$

where $\mathbf{\Psi}(h)$ is the incremental rotation vector, and $\exp[\cdot]$ is the exponential map defined by the Rodrigues formula

$$\exp[\mathbf{\Psi}] = \mathbf{I} + \frac{\sin\|\mathbf{\Psi}\|}{\|\mathbf{\Psi}\|}\hat{\mathbf{\Psi}} + \frac{1-\cos\|\mathbf{\Psi}\|}{\|\mathbf{\Psi}\|^2}\hat{\mathbf{\Psi}}^2 \tag{6}$$

Above, $\mathbf{I}$ is the 3×3 identity operator, $\hat{\mathbf{\Psi}}$ creates the skew symmetric matrix out of a 3-vector $\mathbf{\Psi}$, and $\|\cdot\|$ stands for the Euclidean norm. The rotation vector based representation is singular on spheres $\|\Psi\| = 2\pi n$, $n \in \{1, 2, ...\}$ in the sense that these subsets of the Euclidean 3-space are mapped into the single identity element of the rotation space. Nevertheless, the singularity can be avoided if the incremental formulation is used and the magnitudes of the increments are smaller than 2π. In practice, and specifically for the constrained systems, this is a rather realistic assumption.

In the view of the update formula (5), the finite rotation vector $\mathbf{\Psi}$ can be perceived as belonging to the tangent space $T_{R(t)}SO(3)$. Operations such as vector addition $\mathbf{\Theta}_1 + \mathbf{\Theta}_2$ make sense only if both vectors belong to the same tangent space $\mathbf{\Theta}_1, \mathbf{\Theta}_2 \in T_{R(t)}SO(3)$ *(geometrical consistency)*. When $\mathbf{\Theta}_1 \in T_{R(t)}SO(3)$ and $\mathbf{\Theta}_2 \in T_{R(t+h)}SO(3)$ the differential of the exponential map is employed in order to shift a selected vector from its own tangent space into the tangent space of the other vector. An example is

$$\left(\mathcal{T}^T\mathbf{\Theta}_1\right) + \mathbf{\Theta}_2 \tag{7}$$

where

$$\mathcal{T}[\boldsymbol{\Psi}] = \mathbf{I} + \frac{1-\cos\|\boldsymbol{\Psi}\|}{\|\boldsymbol{\Psi}\|^2}\hat{\boldsymbol{\Psi}} + \frac{\|\boldsymbol{\Psi}\|-\sin\|\boldsymbol{\Psi}\|}{\|\boldsymbol{\Psi}\|^3}\hat{\boldsymbol{\Psi}}^2 \tag{8}$$

was derived for example by Ibrahimbegović *et al.* [6]. As $\hat{\boldsymbol{\Psi}}\boldsymbol{\Psi} = \boldsymbol{\Psi}\times\boldsymbol{\Psi} = \mathbf{0}$, there follows that $\mathcal{T}^T\boldsymbol{\Psi} = \boldsymbol{\Psi}$, which represents a useful fact.

The balance of the angular momentum expressed in the body-frame reads

$$\mathbf{J}\dot{\mathbf{W}} + \mathbf{W}\times\mathbf{J}\mathbf{W} = \mathbf{R}^T\mathbf{t} \tag{9}$$

where $\mathbf{J}$ is the constant referential inertia tensor, $\mathbf{W}$ is the referential angular velocity, and $\mathbf{t}$ is the spatial torque. It is noteworthy that $\mathbf{W}(t) \in T_{\mathbf{R}(t)}SO(3)$, so that an extrapolation $\Psi = h\mathbf{W} + \frac{h^2}{2}\dot{\mathbf{W}}$ makes sense.

Another form of the balance of the angular momentum follows from the spatial formula

$$\frac{d}{dt}(\mathbf{j}\mathbf{w}) = \mathbf{t} \tag{10}$$

where $\mathbf{j}$ is the time-dependent spatial inertia tensor ($\mathbf{j} = \mathbf{R}\mathbf{J}\mathbf{R}^T$), and $\mathbf{w}$ is the spatial angular velocity ($\mathbf{w} = \mathbf{R}\mathbf{W}$). The above expression can be integrated over the time interval $[t, t+h]$ resulting in

$$\mathbf{W}(t+h) = \mathbf{J}^{-1}\exp[-\boldsymbol{\Psi}]\left[\mathbf{J}\mathbf{W}(t) + \mathbf{R}^T(t)\int_t^{t+h}\mathbf{t}dt\right] \tag{11}$$

Discretisations of the above formula give rise to the variety of well-behaved time stepping methods (e.g. Krysl [3]). Nevertheless, an implicit dependence of the incremental rotation vector $\boldsymbol{\Psi}$ on the external torque $\mathbf{t}$ precludes a direct algorithmic analogy with (2).

3 Scheme

The proposed scheme reads

$$\mathbf{R}^{t+\frac{h}{2}} = \mathbf{R}^t\exp\left[\frac{h}{2}\mathbf{W}^t\right] \tag{12}$$

$$\mathbf{T}^{t+\frac{h}{2}} = \left(\mathbf{R}^{t+\frac{h}{2}}\right)^T \mathbf{t}^{t+\frac{h}{2}} \tag{13}$$

$$\mathbf{W}^{t+\frac{h}{2}} = \mathbf{J}^{-1}\left[\exp\left[-\frac{h}{2}\mathbf{W}^t\right]\mathbf{J}\mathbf{W}^t + \frac{h}{2}\mathbf{T}^{t+\frac{h}{2}}\right] \tag{14}$$

$$\mathbf{W}_1^{t+h} = \mathbf{W}^t + \mathbf{J}^{-1}h\left[\mathbf{T}^{t+\frac{h}{2}} - \mathbf{W}^{t+\frac{h}{2}} \times \mathbf{J}\mathbf{W}^{t+\frac{h}{2}}\right] \tag{15}$$

If explicit

$$\mathbf{R}^{t+h} = \mathbf{R}^{t+\frac{h}{2}} \exp\left[\frac{h}{2}\mathbf{W}_1^{t+h}\right] \tag{16}$$

$$\mathbf{W}_2^{t+h} = \mathbf{J}^{-1} \exp\left[-\frac{h}{2}\mathbf{W}_1^{t+h}\right]\left[\exp\left[-\frac{h}{2}\mathbf{W}^t\right]\mathbf{J}\mathbf{W}^t + h\mathbf{T}^{t+\frac{h}{2}}\right] \tag{17}$$

otherwise

$$\textbf{solve}\ \left(\exp\left[\frac{h}{2}\mathbf{W}_3^{t+h}\right]\mathbf{J}\mathbf{W}_3^{t+h} = \exp\left[-\frac{h}{2}\mathbf{W}^t\right]\mathbf{J}\mathbf{W}^t + h\mathbf{T}^{t+\frac{h}{2}}\right) \tag{18}$$

$$\mathbf{R}^{t+h} = \mathbf{R}^{t+\frac{h}{2}} \exp\left[\frac{h}{2}\mathbf{W}_3^{t+h}\right] \tag{19}$$

In the first formula (12) the mid-step rotation $\mathbf{R}^{t+\frac{h}{2}}$ is extrapolated with the forward Euler scheme. It is then used to compute the referential torque components in (13). In equation (14) the idea of LIEMID[E1] algorithm by Krysl [3] is borrowed in order to approximate the mid-step angular velocity $\mathbf{R}^{t+\frac{h}{2}}$. The central difference scheme is applied to the referential angular momentum balance in formula (15). This step is somewhat naive, but we need it in order to preserve the algebraic structure of formula (2). This is also the source of the *geometrical inconsistency*. Due to the collinearity of the incremental rotation vector and the initial angular velocity there holds

$$\mathcal{T}^T\left[\frac{h}{2}\mathbf{W}^t\right]\mathbf{W}^t = \mathbf{W}^t \tag{20}$$

so that the right hand side of (15) resides in the tangent space $T_{\mathbf{R}(t+h/2)}SO(3)$. The left hand side, however, belongs to $T_{\mathbf{R}(t+h)}SO(3)$. Thus, the equality in (15) is not formally rigorous.

In the explicit version of the scheme one would nevertheless like to make some use of $\mathbf{W}_1^{t+h}$. As the right hand side of (15) is in $T_{\mathbf{R}(t+h/2)}SO(3)$, and it is supposed to approximate $\mathbf{W}(t+h)$, one can notionally interpret (15)

as an assignment to $\mathbf{W}_1^{t+h}$ of its own pull-back (along the exponential map) to $T_{\mathbf{R}(t+h/2)}SO\,(3)$. Now formula (19) becomes a "consistent" backward Euler step, updating the mid-step rotation into $\mathbf{R}^{t+h}$. There also holds

$$\mathcal{T}^T\left[\frac{h}{2}\mathbf{W}_1^{t+h}\right]\mathbf{W}_1^{t+h}=\mathbf{W}_1^{t+h} \tag{21}$$

which happens to alleviate the inconsistency (again, this is only a notional trick). The scheme (12-16) has two drawbacks: conservation of the angular momentum is only approximate, and the kinetic energy experiences a positive drift (cf. Section 4). This is remedied in (17), where the angular momentum conservation is algorithmically enforced. As it will be illustrated, the scheme (12-17) has a negative energy drift and becomes strongly dissipative for large time steps.

Although in applications involving small incremental rotations (e.g. constrained systems) the scheme (12-17) will be often sufficient, it is useful to have at hand a refined method, that does not experience the energy drift. Formulae (12-16) are still of use, although $\mathbf{W}_1^{t+h}$ becomes now merely a dummy variable. Equation (15) needs to be stated only to solve for the constraint reactions (which contribute to $\mathbf{T}^{t+\frac{h}{2}}$). After that, the final implicit Euler half-step is executed more rigorously. As the configuration has already been advanced from $\mathbf{R}^t$ to $\mathbf{R}^{t+\frac{h}{2}}$, we do not wish to undo it. Rather, the following mid-point approximation of (11) is exercised

$$\exp\left[\frac{h}{2}\mathbf{W}^t\right]\exp\left[\frac{h}{2}\mathbf{W}^{t+h}\right]\mathbf{J}\mathbf{W}^{t+h}=\mathbf{J}\mathbf{W}^t+h\mathbf{t}^{t+\frac{h}{2}} \tag{22}$$

where the first exponential has already been computed, while the second one implicitly involves $\mathbf{W}^{t+h}$. It should be noted, that the rotation update $\mathbf{R}\,(t+h)=\mathbf{R}\,(t)\exp\left[\mathbf{\Psi}\,(h)\right]$ makes sense, provided $\mathbf{\Psi}\,(h)\in T_{\mathbf{R}(t)}SO\,(3)$. In that respect, while the first update $\mathbf{R}^{t+\frac{h}{2}}=\mathbf{R}^t\exp\left[\frac{h}{2}\mathbf{W}^t\right]$ is correct, the consecutive one $\mathbf{R}^{t+h}=\mathbf{R}^{t+\frac{h}{2}}\exp\left[\frac{h}{2}\mathbf{W}^{t+h}\right]$ might seem inconsistent. More correctly, there should hold

$$\mathbf{R}^{t+h}=\mathbf{R}^{t+\frac{h}{2}}\exp\left[\mathcal{T}^T\left[-\frac{h}{2}\mathbf{W}^{t+h}\right]\frac{h}{2}\mathbf{W}^{t+h}\right] \tag{23}$$

where $\frac{h}{2}\mathbf{W}^{t+h}\in T_{\mathbf{R}(t+h)}SO\,(3)$ was carried over to $T_{\mathbf{R}(t+h/2)}SO\,(3)$ by means of the reverse half-rotation $\mathbf{\Psi}\,(h)=-\frac{h}{2}\mathbf{W}^{t+h}$, and hence $\mathcal{T}^T\left[-\frac{h}{2}\mathbf{W}^{t+h}\right]$. Again, by the collinearity argument, there follows $\mathcal{T}^T\left[-\frac{h}{2}\mathbf{W}^{t+h}\right]\frac{h}{2}\mathbf{W}^{t+h}=\frac{h}{2}\mathbf{W}^{t+h}$. The implicit solve (18) requires few iterations of Newton scheme. The velocity $\mathbf{W}_1^{t+h}$ is used as an initial guess. The final configuration update follows in (19).

In the sequel the scheme (12-16) will be addressed as NEW1, the scheme (12-17) will be addressed as NEW2 and the scheme (12-15, 18-19) will be addressed as NEW3.

4 Stability

Conservation and stability properties are most conveniently analysed in the space of referential angular momenta, $\mathbf{\Pi} = \mathbf{JW}$. Assume, that the external torque $\mathbf{t} \equiv \mathbf{0}$. Conservation of the spatial angular momentum reads then

$$\mathbf{R}(t)\,\mathbf{\Pi}(t) = \mathbf{R}(0)\,\mathbf{\Pi}(0) \tag{24}$$

which together with the conservation of the kinetic energy implies

$$\frac{1}{2}\mathbf{\Pi}^T(t)\,\mathbf{\Pi}(t) = \frac{1}{2}\mathbf{\Pi}^T(0)\,\mathbf{\Pi}(0) \tag{25}$$

$$\frac{1}{2}\mathbf{\Pi}^T(t)\,\mathbf{J}^{-1}\mathbf{\Pi}(t) = \frac{1}{2}\mathbf{\Pi}^T(0)\,\mathbf{J}^{-1}\mathbf{\Pi}(0) \tag{26}$$

where the kinetic energy $E_k = \frac{1}{2}\mathbf{W}^T\mathbf{JW}$. Free rigid rotation can be then viewed as a purely geometrical problem of intersection between the sphere (25) and the ellipsoid (26) in the $\mathbf{\Pi}$-space. In general, the intersection curve is of higher order and cannot be written down in an explicit form. A rotation integrator traces the curve numerically. In particular, let us have a look at formula (15)

$$\mathbf{\Pi}_1^{t+h} = \mathbf{\Pi}^t + h\mathbf{\Pi}^{t+\frac{h}{2}} \times \mathbf{W}^{t+\frac{h}{2}} \tag{27}$$

At any time, $\mathbf{\Pi}(t)$ is normal to the momentum sphere (25) and $\mathbf{W}(t)$ is normal to the energy ellipsoid (26). Hence, the product $\mathbf{\Pi}^{t+\frac{h}{2}} \times \mathbf{W}^{t+\frac{h}{2}}$ can be interpreted as an approximation of the tangent to the intersection curve at $t + h/2$, and (27) becomes a surface intersection tracing scheme. In our case, $\mathbf{\Pi}^{t+\frac{h}{2}}$ is obtained from $\mathbf{\Pi}^t$ by rolling on the surface of the momentum sphere according to the formula

$$\mathbf{\Pi}^{t+\frac{h}{2}} = \exp\left[-\frac{h}{2}\mathbf{W}^t\right]\mathbf{\Pi}^t \tag{28}$$

This is a first order update, as it results from the solution of a linear ordinary equation of rotation about a fixed axis (origin of the exponential map). Hence,

$\mathbf{\Pi}^{t+\frac{h}{2}} \times \mathbf{W}^{t+\frac{h}{2}} = \mathbf{\Pi}\left(t+\frac{h}{2}\right) \times \mathbf{W}\left(t+\frac{h}{2}\right) + O\left(h^2\right)$, where $\mathbf{\Pi}\left(t\right), \mathbf{W}\left(t\right)$ is the exact solution. One can then show, that (27) is of second order. Unfortunately, as the tangent to two convex surfaces is used, points generated by (27) lay outside of both surfaces. Only with $h \to 0$ they approach the actual intersection curve. For large h it is easy to step far outside of both surfaces and rapidly climb up over the increasing energy levels. NEW1 conserves neither the momentum nor the energy and is prone to the catastrophic energy blowup.

By algorithmic enforcement of the momentum conservation (17), the solution iterates cling to the momentum sphere. There holds

$$\mathbf{\Pi}_2^{t+h} = \exp\left[-\frac{h}{2}\mathbf{W}_1^{t+h}\right] \exp\left[-\frac{h}{2}\mathbf{W}^{t}\right] \mathbf{\Pi}^{t} \tag{29}$$

and thus, one always stays on the surface of the conserved momentum. Staying within a compact set prevents an unbounded growth of the energy. The energy blowup is not possible for NEW2. The dissipative behaviour of the scheme however, is not explained by this fact alone. Generally, a sequence of points on a compact set will have at least one accumulation point. Qualitatively, only three types of behaviour are possible (Figure 1):

- *Swelling* of the energy ellipsoid until its smallest radius and the radius of the momentum sphere become equal. The final state corresponds to the stable rotation about the axis of the minimum moment of inertia. This behaviour is typical for first order updates of kind (28), but also for example the explicit scheme by Simo and Wong [2].
- *Shrinking* of the energy ellipsoid until its largest radius and the radius of the momentum sphere become equal. The final state corresponds to the stable rotation about the axis of the maximum moment of inertia. This is the case for NEW2.
- *Oscillation* about the intersection curve of the energy ellipsoid and the momentum sphere. This is the case for NEW3, as well as for many other implicit algorithms [3,5].

Some local analysis of the energy change is typically possible. For NEW2, by the linearisation with respect to the time step, it can be shown that

$$E_k^{t+\frac{h}{2}} - E_k^t \simeq \frac{h^2}{8}\left\langle \hat{\mathbf{\Pi}}^t \mathbf{W}^t, \mathbf{J}^{-1}\hat{\mathbf{\Pi}}^t \mathbf{W}^t \right\rangle \tag{30}$$

and

$$E_k^{t+h} - E_k^{t+\frac{h}{2}} \simeq -\frac{h^2}{8}\left\langle \hat{\mathbf{\Pi}}^t \mathbf{W}^t, \mathbf{J}^{-1}\hat{\mathbf{\Pi}}^t \mathbf{W}^t \right\rangle \tag{31}$$

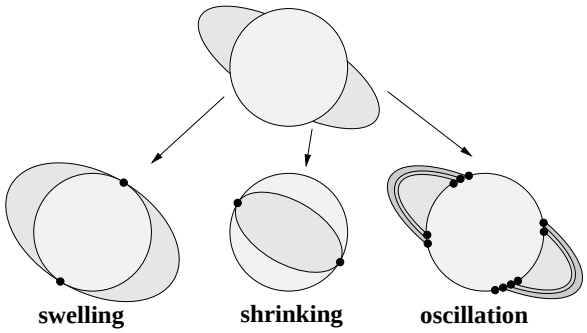

Figure 1. Qualitative behaviour of integration methods enforcing conservation of the spatial angular momentum. Section through the momentum sphere and the energy ellipsoid. The ellipsoid either swells (schemes with positive energy drift), shrinks (schemes with negative energy drift), or oscillates (stable schemes).

where the necessary algebra is somewhat lengthy and has been skipped. The above shows, that up to the second order terms the energy growth and drop cancel out each other. In other words

$$E_k^{t+h} = E_k^t + O\left(h^3\right) \tag{32}$$

This conclusion is not really significant, as it does not imply that NEW2 is a *shrinking* scheme. In fact, the numerical analysis shows that the long term negative drift of NEW2 is overlapped by some up and down oscillations, related to the curvature of the intersecting surfaces. This suggests, that the local analysis of the above kind cannot be conclusive. We do not attempt further analysis. In Sections 7 we resort instead to the numerical examples.

5 Constraints

Very briefly, we comment on the enforcement of constraints and utility of the algebraic structure of equations (2) and (15). Let us rewrite (2) again

$$\mathbf{u}^{t+h} = \mathbf{u}^t + \mathbf{M}^{-1} h \mathbf{f}^{t+\frac{h}{2}} + \mathbf{M}^{-1}\mathbf{H}^T h \Lambda^{t+\frac{h}{2}} \tag{33}$$

Assume, that $\mathbf{u}$ is a column vector composed of angular and linear velocities of all bodies involved in the analysis. Similarly, $\mathbf{M}$ is a block diagonal matrix composed of the relevant inertia operators. The out of balance force $\mathbf{f}$ incorporates the external forcing, and the $\mathbf{W}^{t+\frac{h}{2}} \times \mathbf{J}\mathbf{W}^{t+\frac{h}{2}}$ terms in a suitable manner. Let the configuration $\mathbf{q}$ be composed of the rotation operators $\mathbf{R}$ and the mass centre positions $\bar{\mathbf{x}}$.

Assume now, that a number of *discrete constraints* is given. That is, some local interaction laws has been given between selected pairs of bodies, and

prescribed at a number of spatial points with respect to some *local frames* $\mathbf{a}_i$. Let us rewrite the motion χ of a body in a general form

$$\mathbf{x}(\mathbf{X}, t) = \chi(\mathbf{X}, \mathbf{q}(t)) \tag{34}$$

where $\mathbf{x}$ is the spatial point, $\mathbf{X}$ is the referential point, and $\mathbf{q}$ is the configuration. One can compute the velocity of $\mathbf{x}$ with respect to the spatial base $\mathbf{a}_i$ as

$$\mathbf{U} = \left\{\mathbf{a}^i\right\}^T \frac{\partial \chi(\mathbf{X}, \mathbf{q}(t))}{\partial \mathbf{q}} \mathbf{u} \tag{35}$$

where $\{\mathbf{a}^i\}$ is the 3×3 matrix of column-wise dual-base vectors (cf. [1], Chapter 6). This can be rephrased as

$$\mathbf{U} = \mathbf{H}\mathbf{u} \tag{36}$$

where

$$\mathbf{H} = \left\{\mathbf{a}^i\right\}^T \frac{\partial \chi(\mathbf{X}, \mathbf{q}(t))}{\partial \mathbf{q}} \tag{37}$$

is a linear operator, acting between the spaces of generalised and local velocities $\mathbf{H} : T\mathcal{Q} \to TE^3$. Here, $\mathcal{Q}$ is the configurations space, E^3 is the Euclidean 3-space, and $T\mathcal{Q}, TE^3$ denote the suitable tangent bundles. The operator $\mathbf{H}$ takes a specific form, depending on the underlying kinematic model. Note, that due to the power conjugacy $\langle \mathbf{U}, \mathbf{\Lambda} \rangle = \langle \mathbf{H}\mathbf{u}, \mathbf{\Lambda} \rangle = \left\langle \mathbf{u}, \mathbf{H}^T \mathbf{\Lambda} \right\rangle$, so that the transpose operator acts between the spaces of local and generalised forces $\mathbf{H}^T : T^*E^3 \to T^*\mathcal{Q}$.

Assuming, that all of the local constraint laws can be specified in a velocity-force form, one can write down the general constraints equations as

$$\mathbf{C}(\mathbf{U}, \mathbf{\Lambda}) = \mathbf{0} \tag{38}$$

Now, let the operator $\mathbf{H}$ not only correspond to a single body, but in a suitable manner assemble all of the body and constraint specific $\mathbf{H}$s into a single global form. Hence, $\mathbf{U}$ gathers now in a column-wise manner all of the local velocities, and $\mathbf{\Lambda}$ similarly gathers all of the constraint reactions. Let the mid-step configuration $\mathbf{q}^{t+\frac{h}{2}}$ be obtained by means of (12) for the angular motion, and (1) for the linear motion. Now let $\mathbf{H} = \mathbf{H}\left(\mathbf{q}^{t+\frac{h}{2}}\right)$ and $\mathbf{f}^{t+\frac{h}{2}} = \mathbf{f}\left(\mathbf{q}^{t+\frac{h}{2}}, t + \frac{h}{2}\right)$. Combining (33) and (36), the following saddle point problem results for the

set of all bodies

$$\begin{bmatrix} \mathbf{M} & -\mathbf{H}^T h \\ \mathbf{H} & 0 \end{bmatrix} \begin{bmatrix} \mathbf{u}^{t+h} \\ \mathbf{\Lambda} \end{bmatrix} = \begin{bmatrix} \mathbf{M}\mathbf{u}^t + h\mathbf{f}^{t+\frac{h}{2}} \\ \mathbf{U} \end{bmatrix} \tag{39}$$

where the time indexing by $\mathbf{U}$ and $\mathbf{\Lambda}$ has been dropped for convenience. The Schur complement system can be formed

$$\mathbf{H}\mathbf{u}^{t+h} = \mathbf{H}\mathbf{M}^{-1}\mathbf{H}^T h\mathbf{\Lambda} + \mathbf{H}\left(\mathbf{u}^t + \mathbf{M}^{-1}h\mathbf{f}^{t+\frac{h}{2}}\right) \quad \text{or} \quad \mathbf{U} = \mathbf{D}\mathbf{\Lambda} + \mathbf{B} \tag{40}$$

and the following form of the constraints equations adopted

$$\mathbf{C}\left(\mathbf{D}\mathbf{\Lambda} + \mathbf{B}, \mathbf{\Lambda}\right) = \mathbf{0} \tag{41}$$

In general, the above is a set of nonlinear and sometimes nonsmooth equations, that need to be solved numerically. Many forms of interactions can be casted into this form, including for example the frictional contact constraints [7]. For a single body problem for instance, one can constrain the motion along a specific spatial direction $\mathbf{a}_i$ by demanding $U^i = 0$, and hence obtaining $\Lambda_i = -B^i/W_i^i$. This works well, provided $U^i(0) = 0$. If the initial velocity along the specified direction is nonzero, a single half-step motion of the related point is allowed, introducing an $O(h)$ violation of the constraint.

6 Efficiency

Before resorting to the numerical examples, let us briefly comment on the issue of efficiency. Many of the recently proposed algorithms [3,4,5] posses excellent stability properties and can pursue their tasks with extremely large $O(\pi)$ incremental rotations. The price for those advantages lies in the necessity for solving local implicit problems, for which Newton iterations are usually employed. For large time steps, the local solves involve evaluations of the exponential map at the magnitudes of the rotation angle, for which the truncated Taylor expansion of $\exp[\cdot]$ is not effective. Thus, although sparse steps can be performed, the cost of an individual step is high.

In the explicit multi-body analysis with contacts and joints the possibility of performing $O(\pi)$ steps does not seem practical. The time step has to be small enough in order to capture the geometrical nonlinearities of the multi-body interactions. This is why a lightweight, but well behaved time-stepper is usually a better choice. In this respect, NEW2 involves evaluation of only two

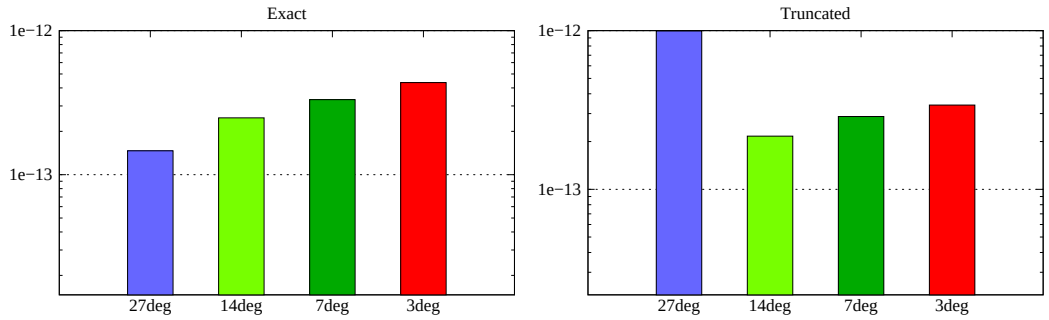

Figure 2. Free rotation. Lose of orthogonality illustrated by the $\left\|\mathbf{I}-\mathbf{R}^T\mathbf{R}\right\|$ norms computed with NEW3 after one million steps with $h \in \left\{\frac{1}{2}, \frac{1}{4}, \frac{1}{8}, \frac{1}{16}\right\}$. The left graph summarises the results computed with the numerically exact routines. The right graph corresponds to the truncated expansion of $\exp[\cdot]$.

exponential maps per step. For small incremental rotations this can be well dealt with by the truncated Taylor expansion of $\exp[\cdot]$.

As the truncated Taylor expansion of $\exp[\cdot]$ has been mentioned above, it is relevant to verify whether the orthogonality of the rotation operator is not compromised. Figure 2 illustrates the norms $\left\|\mathbf{I}-\mathbf{R}^T\mathbf{R}\right\|$ computed with NEW3 after one million steps of the *free rotation* example (given in Section 7.1) at a range of time steps $h = \frac{1}{2}, ..., \frac{1}{16}$. The left graph corresponds to the numerically exact computations (library routines have been used). The right graph corresponds to the same computations, employing the truncated expansion of the scalar terms in (6). It is seen that only for the largest incremental rotation magnitude (27 deg) some lose of orthogonality can be observed. Six terms in the expansions were used.

For long term simulations, where the negative drift of NEW2 cannot be accepted, NEW3 seems to be a good alternative, as it retains the explicitness of the force evaluation and improves upon the stability. Nevertheless, the single implicit problem needs to be solved. In order to evaluate and compare the relative efficiency of the proposed schemes, ten millions time steps of size $\frac{1}{8}$ has been performed for the *free rotation* example given in Section 7.1. Figure 3 summarises the normalised runtimes. The explicit scheme by Simo and Wong [2] computes only one exponential map and hence requires least time. NEW2 with its two exponential map evaluations places itself right after the scheme by Simo and Wong. NEW3 on the other hand takes roughly half of the time needed by Krysl's LIEMID[EA] [3]. This is because the latter method involves solution of two implicit problems per time step.

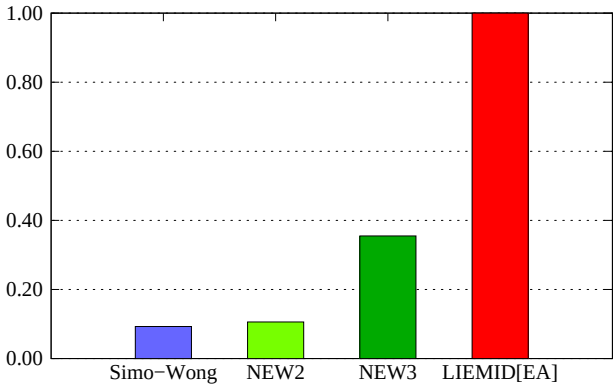

Figure 3. Free rotation. Normalised runtimes comparison for ten millions steps of size $h = \frac{1}{8}$.

7 Examples

The proposed schemes are compared against LIEMID[EA] by Krysl [3], which is one of the best performing schemes today (although its computational cost per time step is considerably higher). In some of the comparisons the explicit scheme by Simo and Wong [2] is also included, as it requires relatively little computational effort per time step. It should be noted that neither the explicit scheme by Simo and Wong, nor LIEMID[EA] comply with the algebraic structure of (2), which from our point of view is a drawback.

7.1 Free rotation

This example is referred to after Krysl [3]. The initial rotation is identity, the initial angular velocity reads $\mathbf{W}^0 = [0.45549, 0.82623, 0.03476]$, and the referential inertia tensor is $\mathbf{J} = \mathrm{diag}\,[0.9144, 1.098, 1.66]$. No external forcing is assumed.

Figure 4 illustrates the magnitudes of the incremental rotation vector computed with NEW3, at a range of time steps. It is seen that small increments of rotation, say $\|\mathbf{\Psi}\| \ll 10\,\mathrm{deg}^{\,2}$, occur for time steps $h < 1/8$. This range of incremental rotations is of the main interest here, although for the sake of illustration this and other examples include larger increments.

Figure 5 illustrates the characteristic momentum phase space behaviour of the proposed schemes. The plots have been obtained over 500 steps of size $h = 1$ (about 55 deg of incremental rotation per time step). Clearly, NEW1 diverges gradually towards the energy blowup. NEW2 dissipates the energy and after

[2] $\|\Psi\| = \left\|\frac{h}{2}\mathbf{W}^t\right\| + \left\|\frac{h}{2}\mathbf{W}^{t+h}\right\|$ is used for the sake of illustration.

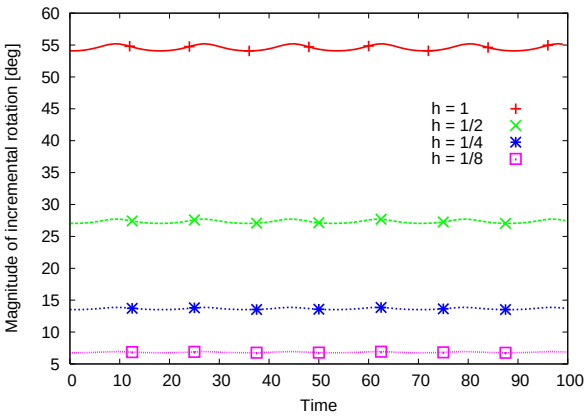

Figure 4. Free rotation. Magnitude of the incremental rotation vector at a range of time steps.

a few tens of steps around the original intersection curve, it switches to the qualitatively new state, asymptotically equivalent to the rotation about the axis of the maximum moment of inertia. NEW3, on the other hand, oscillates stably about the original intersection curve between the momentum sphere and the energy ellipsoid.

Figure 6 illustrates the characteristic energy behaviour of the proposed algorithms. NEW1 experiences a positive energy drift, while NEW2 experiences nearly symmetrical negative energy drift. NEW3, similarly to LIEMID[EA] displays excellent stability although the solution in both cases is oscillatory. NEW3 oscillates on the negative side and with larger amplitude then LIEMID[EA]. The latter method oscillates on the positive side.

Figure 7 illustrates conservation of the spatial angular momentum $\pi = \mathbf{RJW}$. NEW2, NEW3 and LIEMID[EA] clearly conserve the angular momentum (which is their algorithmic feature). On the other hand, NEW1 displays an oscillatory drift for the large time step. For the smaller step, although not visible in the figure, the drift is still present.

Figure 8 illustrates the convergence in the L_2 norm, of the referential angular momentum $\Pi = \mathbf{JW}$ and the rotation operator $\mathbf{R}$. The reference solutions $\mathbf{\Pi}*$ and $\mathbf{R}*$ have been computed with LIEMID[EA] and the time step $h = 2^{-15}$ at time $t = 100$. The solutions $\mathbf{\Pi}(h)$ and $\mathbf{R}(h)$ were computed for time steps $h \in \{1, 2^{-1}, ..., 2^{-10}\}$ at time $t = 100$. It is seen that all of the compared algorithms are second order accurate. All versions of the new scheme outperform the explicit algorithm by Simo and Wong [2]. Interestingly NEW1 displays excellent accuracy of the body-frame angular momentum and performs on a par with LIEMID[EA]. For small time steps the accuracy of the rotation operator obtained with NEW1 also compares well with the one reached by LIEMID[EA].

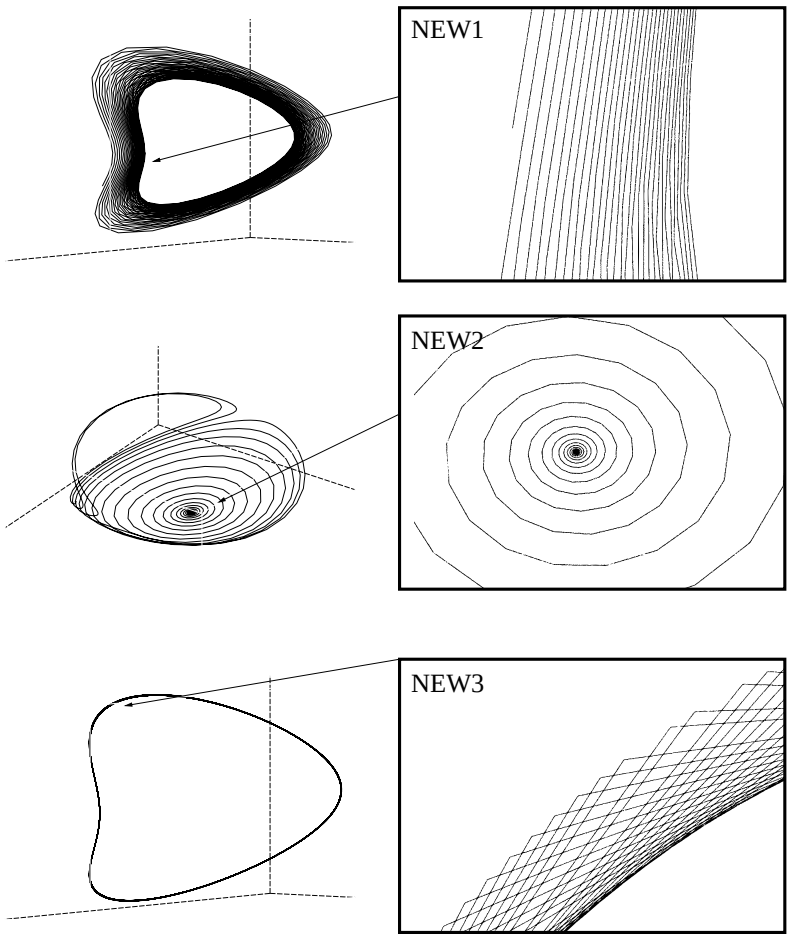

Figure 5. Free rotation. Body-frame angular momentum space plots for 500 steps of size $h = 1$ (about 55 deg of incremental rotation per time step). The large time step allows to capture characteristic behaviour of all three schemes. NEW1 gradually diverges, and it is about to blow up within the next few hundreds of iterations. NEW2 dissipates energy until a stable rotation about the axis of the maximum moment of inertia is reached. NEW3 stably oscillates about the original intersection curve between the momentum sphere and the energy ellipsoid.

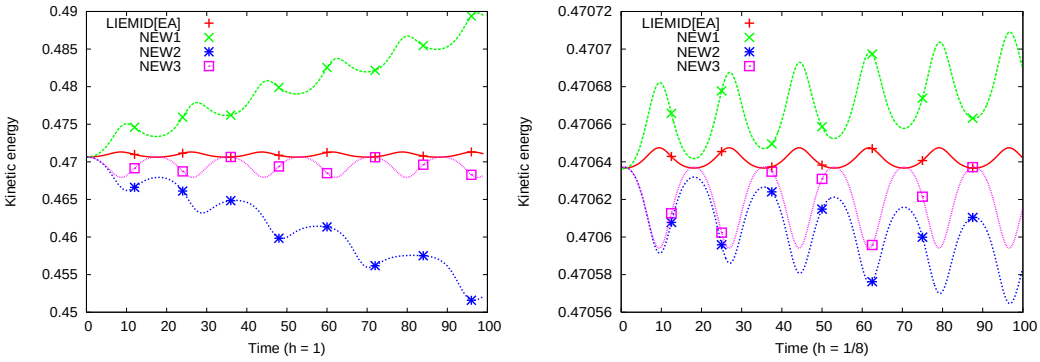

Figure 6. Free rotation. Kinetic energy for step sizes $h = 1$ (left) and $h = 1/8$ (right).

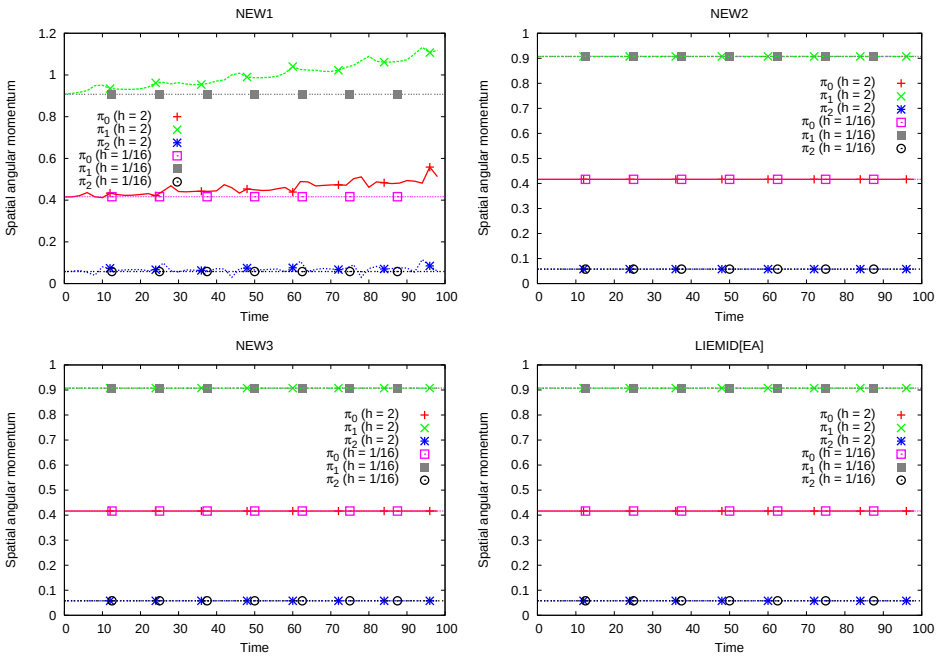

Figure 7. Free rotation. Spatial angular momentum for step sizes $h = 2$ and $h = 1/8$.

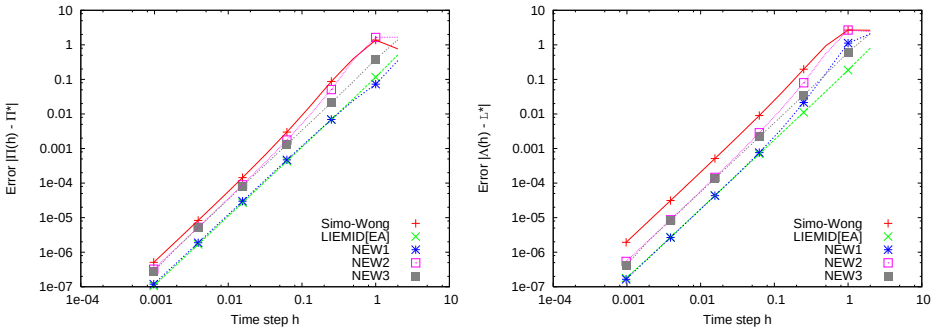

Figure 8. Free rotation. Convergence of the body-frame angular momentum $\mathbf{\Pi} = \mathbf{J\Omega}$ (left), and the rotation operator $\mathbf{\Lambda}$ (right). The reference solutions $\mathbf{\Pi}*$ and $\mathbf{R}*$ have been computed with LIEMID[EA] and the time step $h = 2^{-15}$ at time $t = 100$. The solutions $\mathbf{\Pi}(h)$ and $\mathbf{R}(h)$ were computed for time steps $h \in \{1, 2^{-1}, ..., 2^{-10}\}$.

7.2 Unstable rotation

This example is referred to after Simo and Wong [2]. The example is based on the fact that rigid rotation is stable only about the axes of minimum and maximum moment of inertia (Arnold [8], Chapter 29.2). Small perturbation of rotation around the axis of intermediate moment of inertia leads to unstable oscillation. The initial rotation is identity, the initial angular velocity is zero,

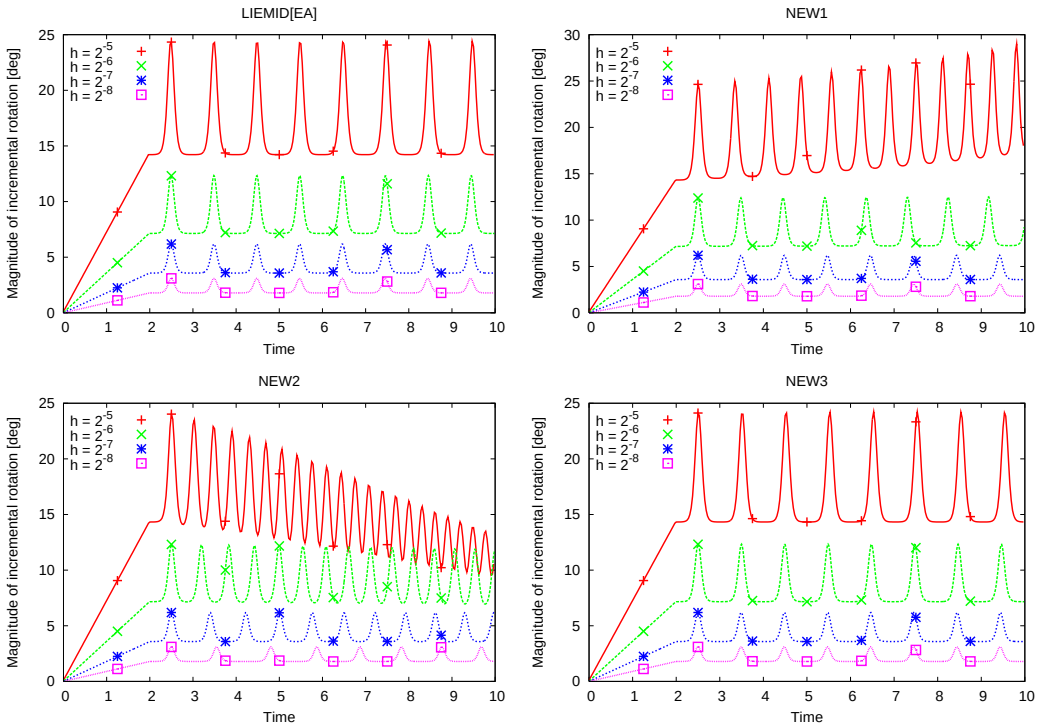

Figure 9. Unstable rotation. Magnitude of the incremental rotation vector for a range of time steps.

and the referential inertia tensor is $\mathbf{J} = \mathrm{diag}\,[5, 10, 1]$. The spatial torque reads

$$\mathbf{t}\,(t) = \begin{cases} [20, 0, 0] & \text{for } 0 \leq t < 2 \\ [0, 1/\,(5h)\,, 0] & \text{for } 2 \leq t \leq 2 + h \\ [0, 0, 0] & \text{for } 2 + h < t \end{cases}$$

so that an impulse inverse proportional to the time step is delivered at $t = 2$. Due to the dependence of torque on the time step, the convergence rate can be only linear for this example. Nevertheless the convergence analysis is included, as this example seems particularly appealing in the context of contact/impact analysis.

Figure 9 compares magnitudes of the incremental rotation vector at the range of time steps from $h = 2^{-5}$ to $h = 2^{-8}$. The characteristic drift properties of the new scheme are clearly visible here. It is seen that the positive drift of NEW1 is smaller than the negative drift of NEW2. At the same time NEW3 gives the best qualitative match withe the results obtained with LIEMID[EA].

Figure 10 illustrates the characteristic energy behaviour at $h = 2^{-5}$ and $h = 2^{-8}$. The energy drift of NEW1 and NEW2 is much smaller in comparison with the one experienced by the explicit scheme by Simo and Wong [2] at the

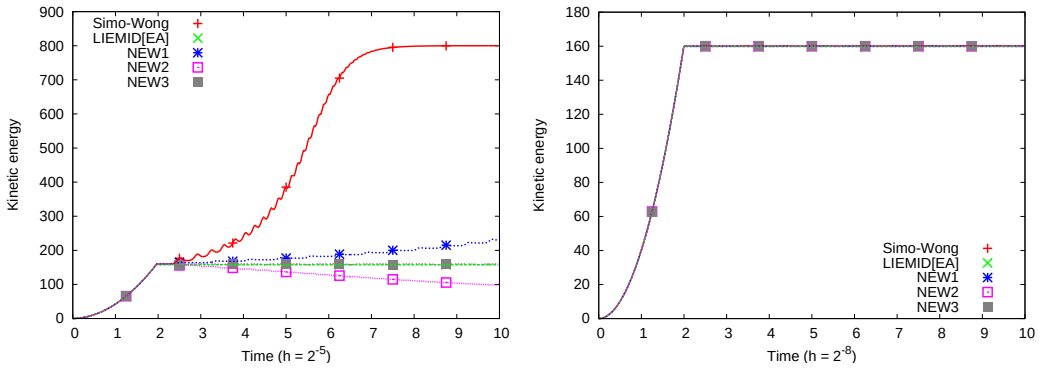

Figure 10. Unstable rotation. Kinetic energy for $h = 2^{-5}$ (left) and for $h = 2^{-8}$ (right).

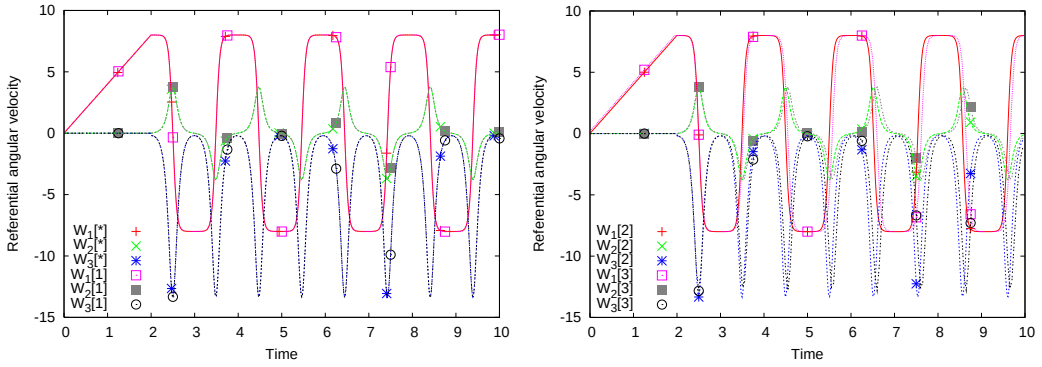

Figure 11. Unstable rotation. Components of the angular velocity in body frame. The $\mathbf{W}\,[*]$ components have been obtained with the explicit scheme by Simo and Wong and $h = 0.001$. The $\mathbf{W}\,[1]$ components have been obtained with NEW1 and $h = 0.01$. Components $\mathbf{W}\,[2]$ correspond to the largest step, for which a qualitatively correct result was obtained with NEW2 ($h = 0.0019$). Components $\mathbf{W}\,[3]$ correspond to the similar result obtained with NEW3 ($h = 0.05$).

larger time step. For the smaller time step all algorithms deliver the solution without a visible drift.

Figure 11 shows the characteristic profile of the body-frame angular velocity. High accuracy of the body-frame variables obtained with NEW1 is confirmed, as the solution obtained with this algorithm at $h = 0.01$ coincides with the reference solution obtained with the explicit scheme by Simo and Wong at $h = 0.001$. It is also visible the the relative accuracy of NEW2 is smaller, as the first qualitatively correct result has been obtained at $h \simeq 0.0019$. NEW3 still gives a qualitatively acceptable result at $h = 0.05$.

Figure 12 illustrates the convergence behaviour. It is noteworthy that the spatial torque formula had to be modified so that the interval $2 \leq t \leq 2 + 0.9h$ was considered for the disturbance impulse. Without this modification LIEMID[EA] consistently delivered very poor results, which is related to the fact that this scheme calculates the torque at the ends of the time in-

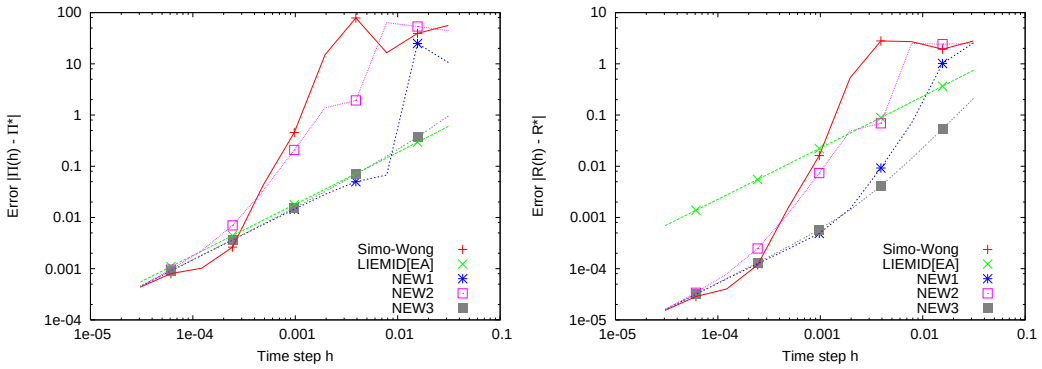

Figure 12. Unstable rotation. Convergence of the body-frame angular momentum $\mathbf{\Pi} = \mathbf{JW}$ (left), and the rotation operator $\mathbf{R}$ (right). The reference solutions $\mathbf{\Pi}*$ and $\mathbf{R}*$ have been computed with the explicit scheme by Simo and Wong and $h = 2^{-22}$ at time $t = 10$. The solutions $\mathbf{\Pi}(h)$ and $\mathbf{R}(h)$ were computed for time steps $h \in \{2^{-5}, 2^{-6}, ..., 2^{-15}\}$.

terval. Again it can be seen that NEW1, NEW3 and LIEMID[EA] perform similarly in terms of the absolute error in the referential angular momentum $\mathbf{\Pi}$, although NEW1 and NEW3 seem much more accurate with respect to the computation of the rotation operator $\mathbf{R}$. As already mentioned, only linear convergence is expected for this example. Nevertheless, the troublesome behaviour of LIEMID[EA] needs to be registered as a matter of future investigation. The reference solution was computed in this case with the explicit scheme by Simo and Wong with $h = 2^{-22}$ at time $t = 10$.

7.3 Heavy top

This is the second example referred to after Simo and Wong [2]. The heavy symmetrical top is spinning around the fixed base point. In this example the applied torque depends on the configuration, introducing additional source of nonlinearity. The top of mass M and axis of symmetry $\mathbf{E}_3$ rotates in the uniform gravitational field $-g\mathbf{e}_3$. The spatial torque reads

$$\mathbf{t} = -Mg\mathbf{r} \times \mathbf{e}_3 \quad \mathbf{r} = l\mathbf{R}\mathbf{E}_3 = \mathbf{R}_{i3}, \;\; i \in \{1, 2, 3\}$$

where the assumed values are $M = 20$, $g = 1$, $l = 1$. As Krysl points out [3], the heavy top model conserves the Hamiltonian

$$H = \frac{1}{2}\pi \cdot \mathbf{j}^{-1}\pi + Mg\mathbf{e}_3 \cdot \mathbf{r}$$

where $\pi = \mathbf{jw}$ is the spatial angular momentum, $\mathbf{j} = \mathbf{RJR}^T$ is the spatial tensor of inertia, and $\mathbf{w} = \mathbf{RW}$ is the spatial angular velocity. In this example

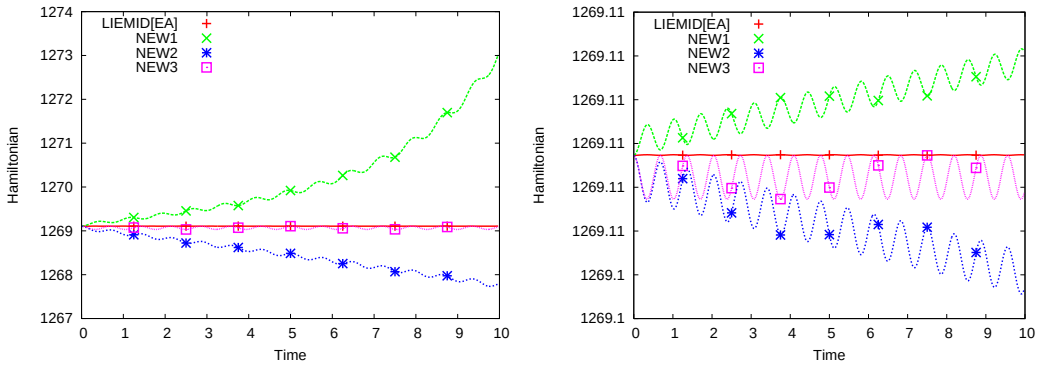

Figure 13. Heavy top. Plots of Hamiltonian for $h = 2^{-5}$ (left) and for $h = 2^{-8}$ (right).

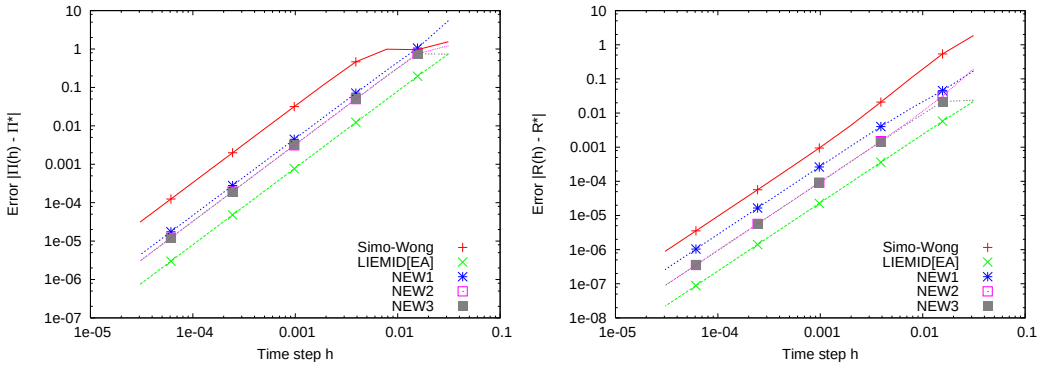

Figure 14. Heavy top. Convergence of the body-frame angular momentum $\Pi = \mathbf{JW}$ (left), and the rotation operator $\mathbf{R}$ (right). The reference solutions $\Pi*$ and $\mathbf{R}*$ have been computed with LIEMID[EA] and $h = 2^{-20}$ at time $t = 10$. The solutions $\Pi(h)$ and $\mathbf{R}(h)$ were computed for time steps $h \in \{2^{-5}, 2^{-6}, ..., 2^{-15}\}$.

the initial rotation is $\mathbf{R}(0) = \exp[0.3, 0, 0]$, the initial angular velocity is $\mathbf{W}(0) = [0, 0, 50]$ and the spatial torque reads $\mathbf{t}(t) = 20[-R_{23}(t), R_{13}(t), 0]$.

Figure 13 illustrates the Hamiltonian history computed with the large time step $h = 2^{-5}$ (nearly $\pi/2$ of rotation increment per step) and the history computed with the smaller step $h = 2^{-8}$ (10 deg rotation increment). The characteristic drift behaviour is visible for the large step, while after the decrease of the time step by the factor of eight, the drift becomes negligible for NEW1 and NEW2. NEW3 behaves stably, although the negative oscillations are clearly pronounced.

Figure 14 illustrates the convergence behaviour. The reference solution was computed with LIEMID[EA] and $h = 2^{-20}$ at time $t = 10$. LIEMID[EA] also clearly outperforms other schemes. All of the proposed algorithms are positioned in between of the explicit approach by Simo and Wong and LIEMID[EA]. NEW2 and NEW3 behave alike and are more accurate in comparison with NEW1.

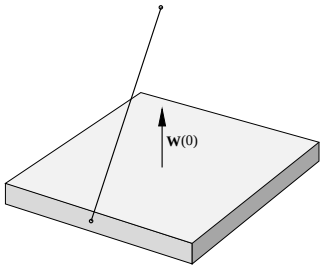

Figure 15. Rotating plate. Rectangular plate with the initial angular velocity $\mathbf{W}(0)$ is constrained by the rigid rod fixed to the centre of the side wall. The other end of the rod rests at a spatial point passing trough the axis collinear with $\mathbf{W}(0)$ and coincident with the mass centre of the plate.

7.4 Rotating plate

In the last example the pendulum comprising a light rectangular plate and a weightless rigid rod is considered (Figure 15). The plate has dimensions $0.2\times0.2\times0.01$ and the length of the rod is $l=\sqrt{0.1}$. In the initial configuration, the rod is fixed to the mass centre of the side wall of the plate at one end. The other end rests at a spatial point placed at distance $h=0.3$ above the mass centre of the plate. The configuration of the plate is $\mathbf{q}=[\mathbf{R},\bar{\mathbf{x}}]$, where $\bar{\mathbf{x}}$ is the spatial placement of the mass centre. The initial configuration reads $\mathbf{q}(0)=[\mathbf{I},\mathbf{0}]$, and the initial angular velocity is $\mathbf{W}(0)=[0,0,50]$. The initial linear velocity is zero. The mass density is $\rho=1$ and the the uniform gravitational field is $-g\mathbf{e}_3$, where $g=9.81$.

The scheme (1-3) is employed for the integration of the motion of the mass centre $\bar{\mathbf{x}}(t)$. The constraint is solved by zeroing the velocity aligned with the rod at time $t+\frac{h}{2}$ (as explained in the last paragraph of Section 5). The mid-step configuration is predicted with (1) and (12). Procedure of this sort was recently discussed by Potra *et al.* [9], although the one applied here is of course much less elaborate.

Figure 16 illustrates the history of the kinetic energy computed over the time interval $[0,10]$ with the time step $h=2^{-10}$ ($\|\Psi\|<10\,\mathrm{deg}$). It is seen that an interaction between the drift of the spatial angular momentum and the imposed constraint results in the considerable loss of energy for NEW1. The momentum conserving schemes NEW2 and NEW 3 pursue the analysis without a visible dissipation.

NEW2 was utilised in order to obtain the time histories of the linear and the angular velocities in Figure 17. Fast rotation around the vertical axis stabilises the plate so that the mass centre oscillates around its initial position.

Figure 18 illustrates the convergence. The reference solution $\mathbf{q}*$ was computed with NEW3 and $h=2^{-22}$ at time $t=1$. The solution $\mathbf{q}(h)$ was computed for

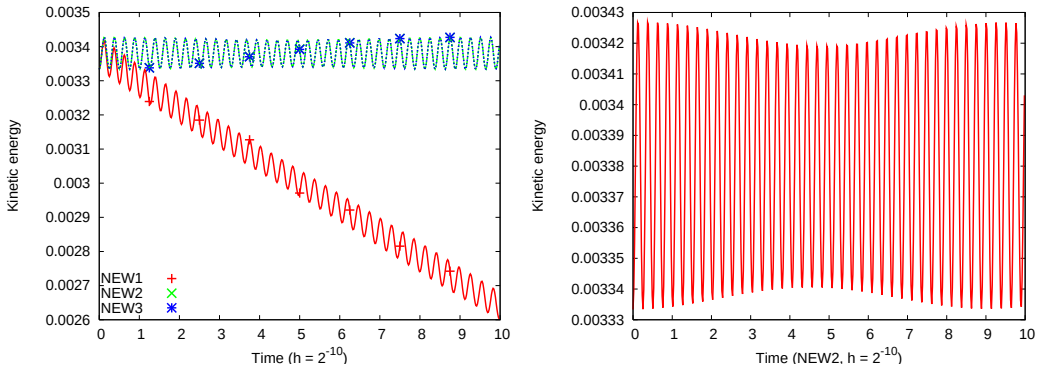

Figure 16. Rotating plate. Kinetic energy computed with $h = 2^{-10}$ by the three proposed algorithms (left), and a closer look at the kinetic energy computed with NEW2 (right).

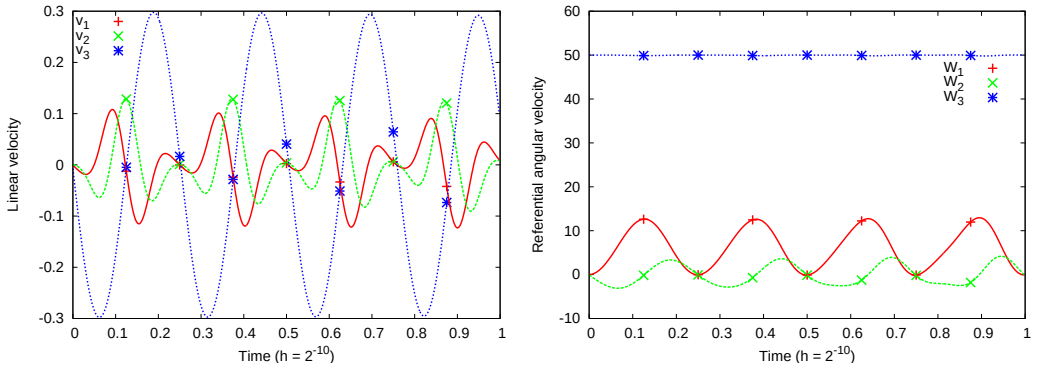

Figure 17. Rotating plate. The linear (left) and the angular (right) velocities over the time interval $[0, 1]$, computed with NEW2 at the time step $h = 2^{-10}$.

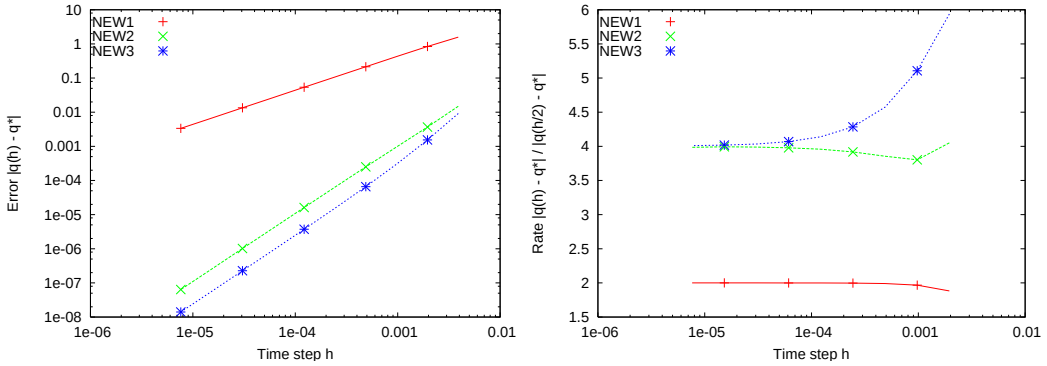

Figure 18. Rotating plate. Absolute error of the configuration $\mathbf{q} = [\mathbf{R}, \bar{\mathbf{x}}]$ (left), and the convergence rate (right). The reference solution $\mathbf{q}*$ has been computed with NEW3 and $h = 2^{-22}$ at time $t = 1$. The solution $\mathbf{q}(h)$ was computed for time steps $h \in \{2^{-8}, 2^{-9}, ..., 2^{-18}\}$.

time steps $h \in \{2^{-8}, 2^{-9}, ..., 2^{-18}\}$. The momentum drift of NEW1 reduces its accuracy to the first order for the considered instance of the constrained motion. NEW2 and NEW3 maintain the second order accuracy. Clearly, NEW3 is the most accurate scheme.

8 Conclusions

Application of the central difference method to the equation of balance of the angular momentum is indeed a naive idea. Nevertheless, the presented schemes possess some appealing properties.

For several reasons NEW2 appears to be well suited for the short to moderate term analysis of constrained systems. As it was shown, the exact conservation of the angular momentum may occur necessary in order to maintain accuracy (Example 7.4). At the same time, the amount of the energy loss is often acceptable for the incremental rotations of magnitudes dictated by an accurate integration of the constrained motion. Additionally, the dissipative behaviour of NEW2 seems advantageous in the context of an explicit multi-body contact analysis, where the episodes of excessively high contact reactions should not render the analysis unstable.

For longer term analysis or for the cases where a higher accuracy is required, NEW3 comes quite handy, with only a moderate increase of the computational cost and still offering all of the advantages of NEW2.

References

[1] Tomasz Koziara. *Aspects of computational contact dynamics.* PhD thesis, University of Glasgow, http://theses.gla.ac.uk/429/, 2008.

[2] K.K. Wong J. C. Simo. Unconditionally stable algorithms for rigid body dynamics that exactly preserve energy and momentum. *International Journal for Numerical Methods in Engineering*, 31:19–52, 1991.

[3] P. Krysl. Explicit momentum-conserving integrator for dynamics of rigid bodies approximating the midpoint lie algorithm. *International Journal for Numerical Methods in Engineering*, 63:2171–2193, 2005.

[4] L. Endres P. Krysl. Explicit newmark/verlet algorithm for time integration of the rotational dynamics of rigid bodies. *International Journal for Numerical Methods in Engineering*, 62:2154–2177, 2005.

[5] William Shelton Jr Phani Kumar, V. V. Nukala. Semi-implicit reversible algorithms for rigid body rotational dynamics. *International Journal for Numerical Methods in Engineering*, 69:2636–2662, 2007.

[6] Adnan Ibrahimbegović, François Frey, and Ivica Kožar. Computational aspects of vector-like parametrization of three-dimensional finite rotations. *International Journal for Numerical Methods in Engineering*, 38:3653–3673, 1995.

[7] M. Jean. The non-smooth contact dynamics method. *Computer Methods in Applied Mechanics and Engineering*, 177(3-4):235–257, 1999.

[8] V. I. Arnold. *Mathematical Methods of Classical Mechanics*, volume 60 of *Graduate Texts in Mathematics*. Springer Verlag, New York, 2^{nd} edition, 1989. 508 pages.

[9] Mihai Anitescu Bogdan Gavrea Jeff Trinkle Florian A. Potra. A linearly implicit trapezoidal method for integrating stiff multibody dynamics with contact, joints, and friction. *International Journal for Numerical Methods in Engineering*, 66:1079–1124, 2006.